



OPEN

Magnitude of the 8.2 ka event freshwater forcing based on stable isotope modelling and comparison to future Greenland melting

Wilton Aguiar^{1✉}, Katrin J. Meissner², Alvaro Montenegro³, Luciana Prado^{4,6}, Ilana Wainer⁴, Anders E. Carlson⁵ & Mauricio M. Mata¹

The northern hemisphere experienced an abrupt cold event ~ 8200 years ago (the 8.2 ka event) that was triggered by the release of meltwater into the Labrador Sea, and resulting in a weakening of the poleward oceanic heat transport. Although this event has been considered a possible analogue for future ocean circulation changes due to the projected Greenland Ice Sheet (GIS) melting, large uncertainties in the amount and rate of freshwater released during the 8.2 ka event make such a comparison difficult. In this study, we compare sea surface temperatures and oxygen isotope ratios from 28 isotope-enabled model simulations with 35 paleoproxy records to constrain the meltwater released during the 8.2 ka event. Our results suggest that a combination of 5.3 m of meltwater in sea level rise equivalent (SLR) released over a thousand years, with a short intensification over ~ 130 years (an additional 2.2 m of equivalent SLR) due to routing of the Canadian river discharge, best reproduces the proxy anomalies. Our estimate is of the same order of magnitude as projected future GIS melting rates under the high emission scenario RCP8.5.

Greenland ice-sheet melting is one of the major responses to the rising atmospheric greenhouse gas concentrations and global mean temperature^{1–3}. The addition of ice-sheet meltwater to the North Atlantic will potentially have a destabilizing effect on the Atlantic Meridional Overturning Circulation (AMOC), which could weaken by more than 70% within the next few centuries^{4–6}. Past meltwater-driven AMOC slowdowns have repeatedly led to millennia-long cold events in the Northern Hemisphere: for example, the Oldest and Younger Dryas (~ 19 to 14.7 kiloyears and 12.9 to 11.7 kiloyears before the present, respectively)^{7–9}. However, the cold event 8.2 kiloyears before present (8.2 ka event hereafter) differs from previous cold events due to its short, century-long duration^{10,11}. The 8.2 ka event also took place in the current interglacial period under boundary conditions that were closer to pre-industrial conditions than earlier cold events¹².

Several freshwater forcing hypotheses involving the Laurentide Ice Sheet (LIS) have been suggested for the 8.2 ka event. These scenarios include three freshwater sources: the drainage of Lake Agassiz¹³, the change in North American continental freshwater routing from LIS retreat^{14,15}, and the on-going retreat of the LIS and its associated meltwater production^{16–18}. The first two sources have relatively well-constrained discharge rates and volumes^{19,20} when compared to the direct ice-sheet meltwater source^{16,17,19,20}. Even though the outburst of Lake Agassiz is commonly considered the main trigger for the 8.2 ka event¹³, recent studies have found that both the LIS retreat and change in the routing of continental discharge might have had a significant role in causing the climate event's anomalies^{15,16,21}, thus raising uncertainties on the role of each of the three meltwater sources in triggering the 8.2 ka event.

The range of estimates of the magnitude of total freshwater release during the 8.2 ka event is also large^{10,11}, ranging from 1.5 to 9 m in equivalent sea-level rise (SLR)^{16,22}. Some of these scenarios were previously used to simulate the cold event with numerical climate models in an attempt to estimate the climatic impacts of the freshwater discharge^{23–25}, and simulation skill was evaluated by comparison with sea surface temperature (SST)

¹Laboratório de Estudos dos Oceanos e Clima, Instituto de Oceanografia, Universidade Federal do Rio Grande—FURG, Rio Grande, RS 96203-900, Brazil. ²Climate Change Research Center and ARC Centre of Excellence for Climate Extremes, University of New South Wales, Sydney, Australia. ³Department of Geography, The Ohio State University, Columbus, OH 43210, USA. ⁴Instituto Oceanográfico, Universidade de São Paulo, São Paulo 05508-120, Brazil. ⁵Oregon Glaciers Institute, Corvallis, OR, USA. ⁶Instituto de Geociências, Universidade de Brasília, Brasília 70297-400, Brazil. ✉email: aguiar.wilton@gmail.com

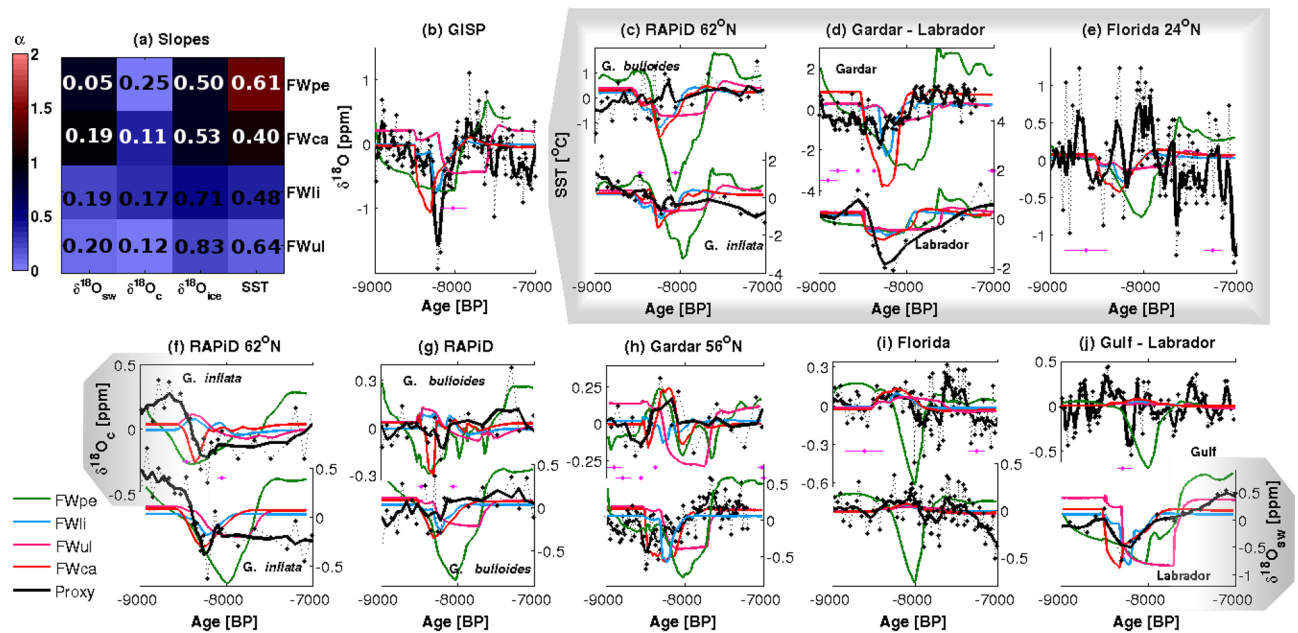


Figure 1. Comparison between time series of proxies and simulations for $\delta^{18}\text{O}_{\text{sw}}$, $\delta^{18}\text{O}_{\text{ice}}$, $\delta^{18}\text{O}_{\text{c}}$ and SST for RAPiD (c,g), Gardar Drift (d,h), Florida Strait (e,i), GISP and Gulf cores (b,j), and slopes and RMSEs (a) in all simulations (locations in Fig. S1 and Table S1). Black dashed and full lines are core values and 2-point moving averages, respectively. Green, blue, magenta and red lines are time series for FWpe, FWli, FWul and FWca. The pink horizontal crosses are the dating (□) and dating errors (—) for the proxies. In (a) RMSE values are plotted in the center of the image while the colors of the squares indicate the values of the slopes. From (f–j), top series are for $\delta^{18}\text{O}_{\text{c}}$, while bottom series are for $\delta^{18}\text{O}_{\text{sw}}$.

reconstructions. Such a large range of meltwater volume is enough to create scenarios ranging from a small change in circulation to a total collapse of the AMOC²⁶. Furthermore, due to a model-dependent stability of ocean overturning, location of deep convection sites and meridional heat transport, the simulated SST response to freshwater forcing varies significantly between distinct simulations^{27,28}. This model dependency makes it difficult to test which freshwater source played the dominant role in triggering the 8.2 ka based on the comparison between the simulated SST response and reconstructed SST changes. However, these uncertainties can be reduced by using a combination of active and non-active tracers, such as oxygen isotopes as well as SSTs.

Constraining the amount of freshwater involved in the 8.2 ka event, and the role of each freshwater source in creating the climate anomalies of the event, will enhance our understanding of the sensitivity of the climate system to freshwater fluxes, which is of obvious importance for future scenarios given the observed recent acceleration of Greenland ice-sheet (GIS) mass loss^{1,2,6}. In this study, we aim to constrain the magnitude and length of freshwater flux that caused the 8.2 ka event. We explore this question by using numerical simulations that calculate both oxygen isotopes, in seawater, in carbonates, and in ice cores, and SSTs prognostically and by comparing the simulations with paleoclimate records of the same variables.

Simulations based on earlier reconstructions

The simulations presented in this section are based on different freshwater release processes that have been suggested in previous studies^{15,18,22,30}. FWpe simulates a scenario where the estimated LIS melting is released exclusively into the Labrador Sea²⁹; FWca represents a scenario where the Canadian continental runoff discharges into the Labrador Sea¹⁵; FWul simulates the melting of the remaining LIS after the collapse of the Hudson Bay's ice saddle²², and FWli simulates a fast rise in sea level surrounding the 8.2 ka event due to prolonged drainage from Lake Agassiz¹⁸ (see “Methods”, “Freshwater forcing for the simulations based on earlier reconstructions” section). SSTs and $\delta^{18}\text{O}$ anomalies from these simulations are then compared with proxy data from 27 locations, at the model's grid cell closest to the geographical coordinates of each core (see “Methods”).

Linear regression slopes and RMSEs for simulated tracers (Fig. 1a) show that FWpe and FWca yield the best estimate of $\delta^{18}\text{O}_{\text{sw}}$ and $\delta^{18}\text{O}_{\text{ice}}$ ($\alpha_{\text{sw}}^{\text{pe}} = 0.89$, $\alpha_{\text{sw}}^{\text{ca}} = 0.99$, $\alpha_{\text{ice}}^{\text{pe}} = 0.86$ and $\alpha_{\text{ice}}^{\text{ca}} = 0.85$). However, FWpe overestimates SST anomalies and estimates a decrease in $\delta^{18}\text{O}_{\text{c}}$ while proxy records point to an increase during this period ($\alpha_{\text{sst}}^{\text{pe}} = 1.43$, $\alpha_{\text{c}}^{\text{pe}} = -0.4$). The FWpe simulation represents the total amount of LIS melting during this period of time, however this flow did not go entirely into the Labrador Sea³⁰. Thus, the overestimation of the SST response could be a result of an overestimation of the total freshwater forcing. Since the model calculates $\delta^{18}\text{O}_{\text{sw}}$ prognostically, and obtains $\delta^{18}\text{O}_{\text{c}}$ using a SST-based transfer function, the misrepresentation of $\delta^{18}\text{O}_{\text{c}}$ is likely due to the SST overestimation. In turn, FWca yields the lowest RMSEs and best slopes across most tracers, with the exception of $\delta^{18}\text{O}_{\text{sw}}$. FWli and FWul have the lowest regression slopes ($\alpha_{\text{all}}^{\text{li}} < 0.3$, $\alpha_{\text{all}}^{\text{ul}} < 0.5$) and highest RMSEs of the four simulations.

(I) Reconstructions				
Experiment	Volume ^a	Duration	Flow (Sv)	References
FWpe	27.1	9–8 ka	0.086	Peltier ³⁰
FWca	8.2	8.5–8.2 ka	0.13	Carlson et al. ¹⁵
FWli	5.3	8.31–8.18 ka	0.13	Li et al. ²²
FWul	9.5	8.2–7.6 ka	0.05	Ullmann et al. ¹⁸
Duration	(II) Flux magnitude (Part A)			
9–8 ka	Sv	0.046	0.066	0.086
8.31–8.18 ka	0.26	FW10	FW11	FW12
	0.19	FW09	FW06	FW03
	0.13	FW07	FW04	FW01
	0.07	FW08	FW05	FW02
Flux	(III) Flux duration (Part B)			
0.066 Sv	Duration	200 years	600 years	1000 years
0.19 Sv	300 years	FW610	FW611	FW612
	130 years	FW67	FW64	FW61
	90 years	FW68	FW65	FW62
	50 years	FW69	FW66	FW63

Table 1. Details of simulations used in this study. The reconstructions table (I) describes the meltwater volumes, fluxes and durations for the homogeneous forcing experiments described in “Simulations based on earlier reconstructions” section. Experiments with hybrid freshwater forcing are separated into Part A and B (II and III). The long meltwater flux in the hybrid experiments in Part A have a fixed duration of 1000 years (9–8 ka), and the short flux is fixed at 130 years (8.31–8.18 ka). FW06 is the simulation in best agreement with proxy data in Part A, so the flux magnitudes of FW06 were used in Part B to test flux duration of the short flux. Note that FW06 is the same simulation as FW61. Volume (^a) is in 10⁵ km³.

The time series of the tracers confirm that FWpe overestimates both the long-term decrease in $\delta^{18}\text{O}$ prior to 8 ka (Fig. 1b,f–i) and the cold SST anomalies (Fig. 1c–e). Analysis of the $\delta^{18}\text{O}$ time series for the remaining simulations show the effect of each discharge in the early-Holocene proxy signal. The routing event in FWca reproduces most of the early-Holocene anomalies recorded between 8.5 and 8.3 ka, especially in the Labrador Sea SST and $\delta^{18}\text{O}_{\text{sw}}$ (Fig. 1d,j), Gardar drift $\delta^{18}\text{O}_{\text{c}}$ (Fig. 1h) and RAPID subsurface (Fig. 1f). The magnitude of the short negative excursion in $\delta^{18}\text{O}_{\text{ice}}$ at 8.2 ka in the GISP2 record is also best reproduced by FWca when compared to the other simulations (Fig. 1b). FWli also reproduces a sharp decrease in $\delta^{18}\text{O}_{\text{ice}}$ at 8.2 ka (Fig. 1b), and in SST and $\delta^{18}\text{O}_{\text{sw}}$ at Gardar drift (Fig. 1d,h), although it underestimates the magnitude of $\delta^{18}\text{O}_{\text{ice}}$ anomalies at 8.2 ka. Finally, the remaining melting of LIS after its collapse simulated in FWul reproduces the stable low $\delta^{18}\text{O}_{\text{c}}$ values at subsurface in the RAPID core (Fig. 1f).

Thus, simulated $\delta^{18}\text{O}$ shows that FWpe, FWca, FWli, and FWul reproduce different parts of the early Holocene signal. This suggests that a realistic freshwater flow for prompting the 8.2 ka event anomalies requires a combination of a long-term meltwater flux with a short-term flux intensification, possibly due to a change in routing of continental runoff and draining of Lake Agassiz²¹.

Hybrid simulations

The simulations analyzed in this section (called hybrid hereafter) follow more complex freshwater release scenarios, testing the range of uncertainties in freshwater flux magnitude and duration as well as changes in freshwater forcing over time. In one set of the hybrid simulations (Table 1, Part A), the freshwater forcing is separated into two components: one lasts longer (1000 years background flux) with relatively low magnitudes (0.086 Sv, 0.066 Sv, and 0.046 Sv), while the other is shorter (130 year-long flux intensification) with relatively high magnitudes (0.13 Sv, 0.07 Sv, 0.19 Sv and 0.26 Sv). A comparison between the short fluxes in the Part A simulations (Fig. 2a–d) shows that a flux intensification of 0.19 Sv achieves the lowest RMSEs in $\delta^{18}\text{O}_{\text{sw}}$, $\delta^{18}\text{O}_{\text{c}}$ and $\delta^{18}\text{O}_{\text{ice}}$ when compared with simulations with the same background flux but different short fluxes (Table S2). In turn, when comparing the long fluxes in the Part A simulations (Fig. 2a–d, columns), it is noticeable that the simulations with 0.066 Sv of background flux have the lowest RMSEs and slopes closest to 1 for SST, $\delta^{18}\text{O}_{\text{c}}$ and $\delta^{18}\text{O}_{\text{ice}}$. Thus, the comparisons based on RMSEs and slopes suggest that a background flux of 0.066 Sv and a short flux of 0.19 Sv best represent the tracer anomalies (simulation FW06—Table S2).

The Part B experiments were aimed at evaluating model sensitivity to the duration of the freshwater forcing. This was accomplished by adopting freshwater flux magnitudes from FW06, the experiment that best represented 8.2 ka event anomalies in Part A, and varying the durations of the individual phases of freshwater addition. The length of the shorter flux in this set of simulations varies from 50 to 300 years, while the longer flux varies from 200 to 1000 years (Table 1).

Simulations FW61 and FW63 show the best match with proxy data with slopes closest to 1 and consistently low RMSEs (Fig. 2e–h, Table S3). Further testing the similarity between the simulated and core time series of $\delta^{18}\text{O}$ in a Taylor diagram allows for a more detailed comparison between simulations. All correlation values in

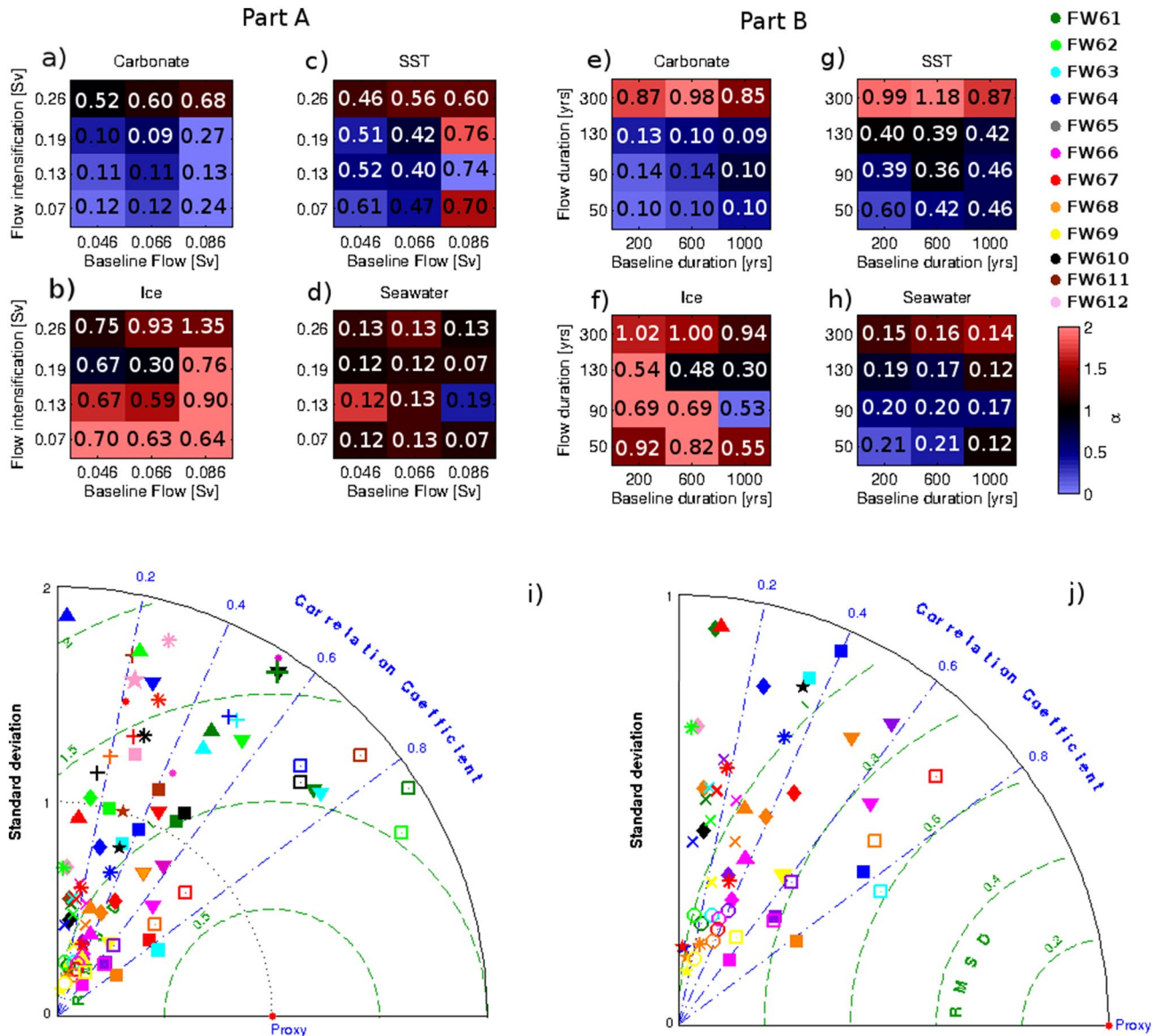


Figure 2. Analysis of simulations in Table 1—Parts A and B. (a) to (h) are the slope and RMSE values for each experiment. Plots (a–d) are for experiments in part A, while plots (e–h) are for experiments in part B. The colour of the squares represents the slopes according to the color bar, and RMSE values are indicated in the center of each cell. (i) Taylor diagram for comparison between proxy and simulated time series of $\delta^{18}\text{O}$ anomalies: GISP ice core (filled square), Rapid Core $\delta^{18}\text{O}_c$ in *G. inflata* (filled rhombus) and *G. bulloides* (plus), Gardar Drift core $\delta^{18}\text{O}_c$ for *G. bulloides* (filled circle), Florida Strait core $\delta^{18}\text{O}_c$ for *G. ruber* (X), Gulf core $\delta^{18}\text{O}_c$ for *G. ruber* (star), Rapid Core $\delta^{18}\text{O}_{sw}$ in *G. inflata* (asterisk) and *G. bulloides* (filled triangle), Gardar Drift core $\delta^{18}\text{O}_{sw}$ (filled inverted triangle), Florida Strait core $\delta^{18}\text{O}_{sw}$ (open circle), and $\delta^{18}\text{O}_{sw}$ in Labrador Sea core (open square). The colors represent different simulations. Taylor diagram (j) is the same as (i), but zoomed in closer to the 0. Standard deviations are normalized by the core value, while RMSE is centered.

the Taylor diagram are statistically significant ($p < 0.05$, $n > 1000$ —Fig. 2i,j). The highest correlations for $\delta^{18}\text{O}_{sw}$ are for the Labrador Sea cores and simulations FW61 (0.84), FW62 (0.88), and FW63 (0.83). In the Gardar Drift time series of $\delta^{18}\text{O}_{sw}$, FW61 and FW63 have the strongest correlation with the core (both 0.75), but the lowest RMSE value is achieved by FW66 (0.76‰). FW61 and FW63 also have the highest positive correlations for $\delta^{18}\text{O}_{sw}$ at the RAPiD core based on *G. bulloides* (0.47 and 0.48 respectively), for *G. bulloides* $\delta^{18}\text{O}_c$ in the RAPiD core (0.54 for FW61). According to the Diebold-Mariano test, RMSEs for FW61, FW63 and FW66 in $\delta^{18}\text{O}_c$ and $\delta^{18}\text{O}_{sw}$ are significantly different with confidence varying from 85 to 99%. The exceptions are $\delta^{18}\text{O}_c$ errors between FW61 and FW63, which are equal with 90% confidence. These results suggest that errors in $\delta^{18}\text{O}_{sw}$ for simulations FW61, FW63 and FW66 are statistically different and possibly not random. Simulations FW61, FW63 and FW66 are the ones that best reproduce $\delta^{18}\text{O}$ mean anomalies in most proxies and locations and have the best correlations and RMSEs for the whole time series. As a last step, and in an effort to determine the most

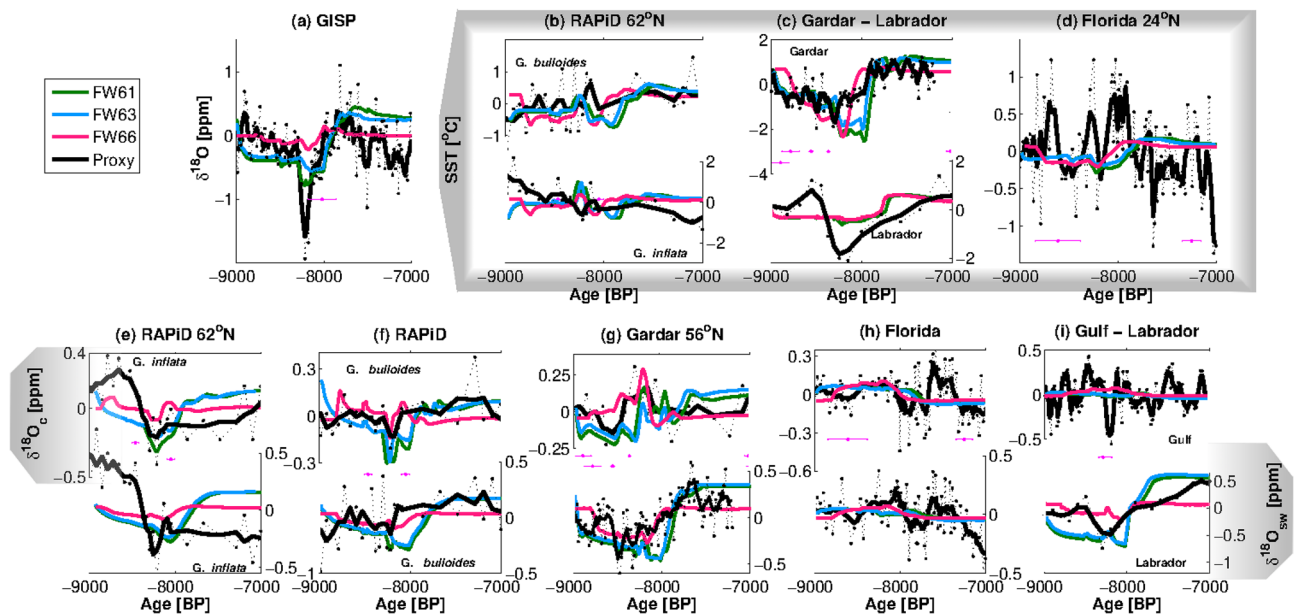


Figure 3. Comparison of simulated and reconstructed $\delta^{18}O_{sw}$, $\delta^{18}O_c$, $\delta^{18}O_{ice}$ and SST time series for the three best fitting hybrid models: RAPiD (b,e,f), Gardar Drift (c,g), Florida Strait (d,h), GISP $\delta^{18}O_{ice}$ (a), Gulf Strait $\delta^{18}O_c$ (i-top) and Labrador Sea $\delta^{18}O_{sw}$ (i-bottom) and SST (c-bottom). Black dashed and full lines are core values and 2-points moving average. Green, cyan, and magenta lines show FW61, FW63, and FW66 simulations, respectively. The pink horizontal crosses are the dating (⊖) and dating errors (↔) for the proxies.

realistic freshwater forcing, we will compare the time series produced by the three best fitting simulations with the proxy reconstructions at the six locations with high resolution data (Fig. 3).

Simulated $\delta^{18}O_{sw}$ and $\delta^{18}O_c$ for FW61/62/63 at the location of the RAPiD core now capture the magnitude of proxy anomalies for *G. bulloides* (Fig. 3f). FW61 and FW63 also reproduce the magnitude of the anomalies at the Gardar Drift core in the *G. bulloides* time series of $\delta^{18}O_c$ and $\delta^{18}O_{sw}$ (Fig. 3g), and the SST time series at the RAPiD location (Fig. 3b-top), and Gardar Drift (Fig. 3c-top).

GISP2 $\delta^{18}O_{ice}$ is best simulated by FW61, which reproduces both the long-term oxygen isotope decrease and the timing of the short-lived decrease at 8.2 ka (Fig. 3a-top). Neither simulated $\delta^{18}O_c$ in the Gulf of Mexico or SSTs in the Strait of Florida show significant variability (Fig. 3d,h,i-top). Taking into account that FW61 exhibits the best match to SST and $\delta^{18}O$ in the proxy record, while also reproducing the GISP2 $\delta^{18}O_{ice}$, we conclude that this simulation is the best representation of the 8.2 ka event in our study.

Discussion

Our first set of simulations evaluate how well different freshwater sources to the North Atlantic reproduce ocean anomalies associated with the 8.2 ka event. Although FWca represents only one of these sources, i.e., a runoff routing event¹⁵, it yields the lowest RMSEs, best slopes and the best representation of most cores time series. This points to the routing event being one of the main contributors to the changes captured by the proxies during the early Holocene. Given that the regression slopes for FWul are significantly lower than for FWca, melting of the remaining LIS after its collapse (FWul) likely only played a background role in creating the climate anomalies at the 8.2 ka, while the routing event (FWca) had much more impact.

We then conducted several additional meltwater flux experiments in order to answer the following question: What magnitudes and rates of freshwater fluxes are most consistent with the 8.2 ka event proxy anomalies? The short 8.2 ka event anomalies recorded in $\delta^{18}O$ climate archives are best reproduced with a simulation forced by a freshwater flux intensification of 0.19 Sv lasting for 130 years. This is in line with earlier simulations performed with the Community Climate System Model version 3, which reproduced the 8.2 ka SST anomalies with 0.13 Sv of freshwater discharge for 99 years²⁴. Here, we show that a higher discharge estimate of 0.19 Sv embedded in a background flux of 0.066 Sv is able to reproduce $\delta^{18}O$ anomalies in addition to SST anomalies.

Based on 35 $\delta^{18}O$ and SST records from 27 different locations, we consider that our FW61 simulation was able to accurately reproduce the major trends and anomalies recorded in the proxy records for the 8.2 ka event and early-Holocene (Fig. 3). The FW61 simulation suggests that anomalies similar to those associated with the event could have been caused by a total meltwater addition of 7.5 m in SLR equivalent between 9–8 ka, with a short period of intensified flooding, equivalent to a SLR of 2.2 m (included in the 7.5 m estimate), between 8.31 and 8.18 ka (Figs. 4a,b, S2). This short intensification of the freshwater flux in FW61 has similar magnitude as the relative SLR in Southwest Scotland (1.45 m within 300 and 500 years)³¹, but the absolute value for our estimate is 0.75 m higher. This discrepancy could be explained by either local land uplift due to glacial isostatic adjustment over Scotland³², or by a combination of LIS melting and Canadian basin routing, since the routing would not contribute to eustatic SLR. The intensification in freshwater input of 2.2 m also matches previous eustatic

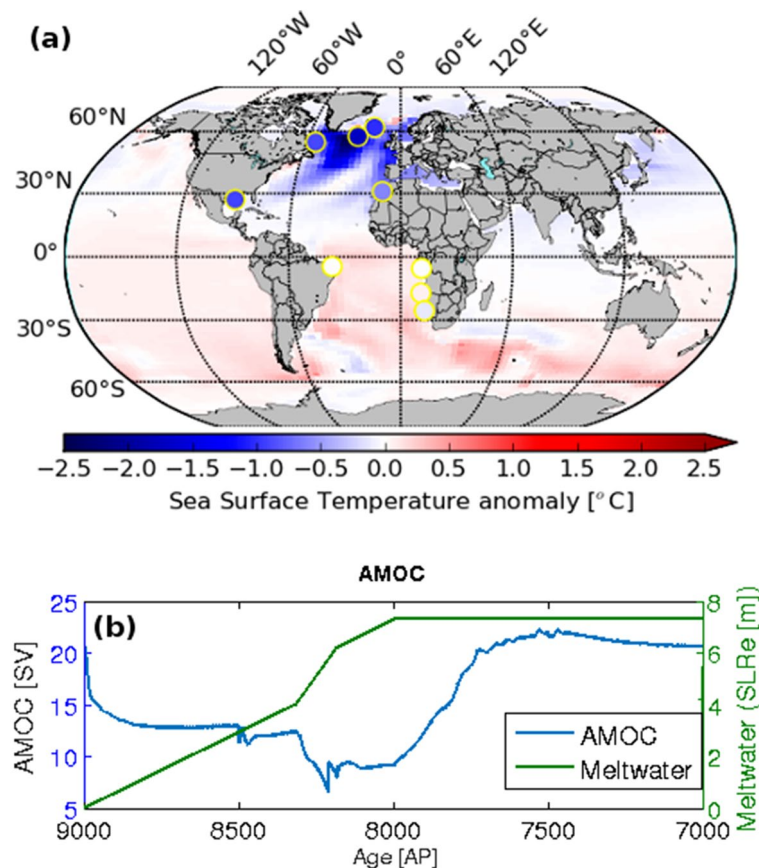


Figure 4. Climate impacts for the hybrid simulation FW61. **(a)** Proxy and model SST anomalies for the FW61 simulation. The color of the circles is plotted according to the anomaly value of the reconstructed SSTs. **(b)** Simulated maximum overturning streamfunction for the North Atlantic as a measurement for the Atlantic Meridional Overturning Circulation (right, blue line), and meltwater added in the FW61 experiment, in Sea Level Rise equivalent (SLRe, green line). Map **(a)** drawn by Wilton Aguiar on Python v2.7 (<https://www.python.org/download/releases/2.7/>).

SLR estimates from the Netherlands (3 ± 1.2 m within 200 years)³³ and Mississippi delta (0.8–2.2 m within 130 years)²². Estimates of SLR rates on longer time-scales for the early-Holocene however differ considerably from ours. Rates of $17.9 \text{ mm year}^{-1}$ (8600–7100 BP), and 24 mm year^{-1} (extending up to 8948–8206 BP) are recorded on the coast of Germany³⁴ and Norway³⁵, much higher than our 7.5 mm year^{-1} estimate. Because the melting of Antarctic Ice Sheet contributed to less than 3 cm of SLR in early-Holocene⁵¹, this difference in meltwater fluxes likely derives from LIS additional melting. This is expected since the meltwater volume in this study is an estimate of the meltwater that was added to the Labrador Sea, part of which was then advected to deep water formation sites, thus affecting large-scale ocean circulation and climate. Additionally, meltwater from the LIS in the early-Holocene was discharged into wide regions in the Arctic and North Atlantic and thus account for a total volume higher than the one we find here³⁰. Therefore, our estimate does not represent the total LIS melting and corresponding SLR for this time span. Neither FW61 nor the proxy records show a clear 8.2 ka response in the Florida Strait (SST). The 8.2 ka event might therefore not have had a significant and far-reaching impact on the Florida Strait region, causing a climate response within model or proxy data background variability. A simulation of the 8.2 ka event with the Hadley Centre Coupled Model, version 3 (HadCM3) also did not reproduce any measurable SST anomalies in the Gulf of Mexico³⁶, thus suggesting that the core SST signal in that location is likely not due to meltwater forcings involved in the 8.2 ka event. The AMOC response to the 8.2 ka freshwater forcing is still debated in the scientific community. In our best-fitting FW61 simulation, AMOC weakens by 62% (13 Sv, Fig. 4b) without collapsing, supporting earlier evidence of substantial AMOC weakening without a collapse during the 8.2 ka event^{37,38}. Matero et al.³⁶ find that AMOC weakens by 55% of its initial overturning, similar to our estimate, based on simulations with the HadCM3.

Implications

The magnitude of the simulated climate change during the 8.2 ka event offers a pertinent reference point for future climate trends¹². The Greenland Ice Sheet is undergoing considerable melting and this is likely to continue well into the future^{1,29}. Greenland melting scenarios for the next millennium project SLR of 7.28 m for the RCP8.5 scenario of the Intergovernmental Panel on Climate Change³⁹. Current meltwater fluxes from the Greenland Ice

Sheet are estimated to be ~ 0.005 Sv²⁹. Even though this flux is considerably smaller than the ones used in our experiments, projections of freshwater flux intensification for the next centuries are similar to the FW61 baseline flows. For example, Golleger et al.⁶ found an increase in freshwater flux from Greenland ice-sheet melting of 0.015 Sv by 2100 in the RCP8.5 scenario. Lenaertes et al.⁴⁰ project an acceleration of the meltwater flux from Greenland up to 0.08 ± 0.003 Sv by 2200, while the maximum melting scenario of Aschwanden et al.³⁹ projects a flux exceeding 0.17 Sv by 2300 ($15 \text{ mm of SLR year}^{-1}$). Bakker et al.⁴ found a median discharge higher than 0.08 Sv by the year 2300. The projected input of freshwater into the North Atlantic associated with the RCP8.5 scenario is therefore of the same magnitude as those in the FW61 simulation in terms of total SLR contribution (7.5 m), duration (1000 years) and flux magnitude (0.066 Sv to 0.19 Sv). However, it is important to highlight that future emission scenarios also include intensive surface radiative warming, which will add to the stratification effect and thus intensify the future overturning weakening²⁸. Additionally, future GIS meltwater will likely flow into the coastal areas surrounding the ice sheet, instead of exclusively into the Labrador Sea³⁹, and thus, its impact on the ocean overturning will potentially differ from the focused meltwater injection in the Labrador during the 8.2 ka event. Moreover, the climate response to an increase in meltwater will be in addition to the much greater warming response due to increasing greenhouse gas concentrations, as well as changes due to topography and albedo changes over Greenland. Nevertheless, the estimated meltwater flux from the GIS in the not too distant future is comparable to the fluxes we find as the forcing behind the 8.2 ka event.

Methods

Model and data. Simulations were performed using the University of Victoria Earth System Climate Model version 2.9 (UVic Model)⁴¹, with the addition of oxygen isotopes^{42,43}. Water in the ocean, atmosphere, sea-ice, and on land is compartmentalized into ^{18}O and ^{16}O to allow the estimation of $\delta^{18}\text{O}$ distribution^{42–46}. A detailed description of the experimental setup is given in the Supporting Information. We compared simulated $\delta^{18}\text{O}$ and SSTs to paleoclimate record mean anomalies for the 8.2 ka event (averaged between 7.9 and 8.5 ka—Supplementary) and time series from six locations (Fig. S1-stars). Mean anomalies of oxygen isotope ratios in seawater ($\delta^{18}\text{O}_{\text{sw}}$), carbonate ($\delta^{18}\text{O}_{\text{c}}$), ice ($\delta^{18}\text{O}_{\text{ice}}$), and SSTs, were taken from Morrill et al.⁴⁷. These proxy anomalies are based on data from 27 cores (Fig. S1), some recording more than one paleoclimate proxy. Overall, our analysis includes ten SST records, ten $\delta^{18}\text{O}_{\text{sw}}$ records, seven $\delta^{18}\text{O}_{\text{c}}$ records and eight $\delta^{18}\text{O}_{\text{ice}}$ records. The mean anomalies in the simulations are calculated following the methodology by Morrill et al.⁴⁷. They are defined as the difference between SST (or $\delta^{18}\text{O}$) values averaged between 7.9 and 8.5 ka and their climatological mean, only for values above (or below) the mean plus (minus) two standard deviations. The climatological mean is defined as the average between 9 and 7 ka, excluding the period between 7.9 and 8.5 ka.

For most records, the simulated values were taken at the model's grid cell closest to the geographical coordinates of each core, at the surface level of the ocean model (17.5 m). The tracers reconstructed from *Globorotalia inflata* were compared to the simulated ocean tracers averaged between 82.5 and 177.5 m, due to the wide range of vertical migration inherent to this species. Thus, time series for the RAPiD core based on *Globigerina bulloides* reflect surface changes, while those based on *G. inflata* reflect changes in the upper thermocline. The UVic model does not simulate isotopic fractionation during foraminiferal calcification. Thus, model $\delta^{18}\text{O}_{\text{c}}$ was estimated by an SST-based transfer function^{48,49}.

In order to evaluate the simulations' skill in reproducing the reconstructed $\delta^{18}\text{O}$, the linear regression's slope (α) and Root Mean Square Errors (RMSE) were calculated for the model anomalies using proxy anomalies as reference. Equality between model and proxy happens when $\alpha = 1$. For the time series, centered RMSE, normalized standard deviations and Pearson's correlations were compared in a Taylor diagram in order to evaluate the performance of the simulations in reproducing the proxy time series. To assure that the difference of the RMSEs for the time series of $\delta^{18}\text{O}_{\text{sw}}$ and $\delta^{18}\text{O}_{\text{c}}$ are significant, we performed a Diebold-Mariano test^{50,51} between each of the experiments in Part B. We then report the Diebold-Mariano test results and its significance level for the simulations with the best performances. All remaining values of the Diebold-Mariano test and its critical confidence percentages are presented in the Supplementary Information (Supplementary S2). More information on the experimental setup and core data can be found in the Supplementary Material.

Freshwater forcing for the simulations based on earlier reconstructions. There are four main estimates of freshwater input into the North Atlantic close to the time of the 8.2 ka event. A glacial isostatic adjustment model by Peltier³⁰ estimates that $27.1 \times 10^5 \text{ km}^3$ of freshwater were added to the North Atlantic from LIS retreat from 9 to 8 ka. The meltwater from LIS estimated by Peltier³⁰ did not flow entirely into the Labrador Sea, so this estimate can be used as an upper constraint for total meltwater discharged in the Labrador Sea in the period. Carlson et al.¹⁵ estimate a $0.13 \text{ Sv} \pm 0.03 \text{ Sv}$ increase in the inflow of freshwater into Labrador Sea after the collapse of Hudson Bay that ended $\sim 8.2 \text{ ka}$ ¹⁸ due to the routing of the western Canadian Plains runoff ($8.2 \times 10^5 \text{ km}^3$ in volume). Although the routing event does not contribute to SLR, it would still alter the oxygen isotope ratios and surface water buoyancy in the Labrador Sea, thus potentially affecting deepwater formation rates. Li et al.²² found a $1.5 \pm 0.7 \text{ m}$ of eustatic SLR between 8.31 ka and 8.18 ka ($5.3 \times 10^5 \text{ km}^3$ in volume) from a SLR reconstruction, which includes the freshwater release from the lake outburst. Ullman et al.¹⁸ estimate that additional melting of the LIS after its collapse contributed to $3.6 \pm 0.4 \text{ m}$ of SLR that began $\sim 8.2 \text{ ka}$ and ended $7.6 \pm 0.6 \text{ ka}$ ($\sim 9.5 \times 10^5 \text{ km}^3$ in volume). The estimated Antarctic Ice Sheet contribution to SLR during the early-Holocene is lower than 3 cm, i.e. substantially smaller than LIS⁵¹, so no meltwater was added in the Southern Hemisphere in the simulations. Using these estimates, we derived four main freshwater release experiments running from 9 ka until 7 ka (Table 1, (I) Reconstructions).

It is important to highlight that the four freshwater release estimates refer to different processes, and thus each simulation will represent the effect of a specific process in creating proxy anomalies of the 8.2 ka event:

FWca represents the Canadian Plains routing event, FWul represents the effect of meltwater from the remaining LIS after its collapse, FWli represents the effect of the total freshwater addition to the ocean surrounding the 8.2 ka event (not accounting for routing events), and FWpe represents the total early-Holocene meltwater from the LIS. By simulating these separately, we estimate the signature of each process on the $\delta^{18}\text{O}$ and SST records.

In our simulations, all freshwater was added to the Labrador Sea (50°N – 65°N ; 70°W – 35°W). Meltwater from the LIS and Lake Agassiz are estimated to have had a $\delta^{18}\text{O}$ varying from -24 to -25‰ during the early-Holocene^{52,53}; we therefore added freshwater with a $\delta^{18}\text{O}$ of -25‰ . Overturning in FWpe collapsed after 8 ka; to restart the North Atlantic deep convection smoothly a virtual salt flux decreasing from -0.2 to -0.05 Sv (8 ka until 7.5 ka) with no isotopic signature was added.

Freshwater forcing of the hybrid scenarios. In addition to this first set of simulations, which are based on earlier geological reconstructions and described in “[Freshwater forcing for the simulations based on earlier reconstructions](#)” section, we also integrated additional sensitivity simulations. Twenty-four experiments were performed based on the uncertainty ranges of the Peltier³⁰, Li et al.²², and Carlson et al.¹⁵ estimates (Table 1). The 7.5 m in SLR equivalent estimated by Peltier³⁰ was not fully released into the Labrador Sea. In turn, Li et al.³⁰ estimated the date of the meltwater outburst within 8.245 ± 0.065 ka and their flux estimate has a 0.06 Sv uncertainty. Additionally, the Canadian continental basin routing event from Carlson et al.¹⁵ likely contributed to an enhancement of freshwater flow to the Labrador Sea of 0.13 Sv lasting up to 300 years. Together, these result in potential freshwater fluxes varying between 0.046 and 0.26 Sv and lasting between 200 and 1000 years. With these experiments, called “hybrid”, we test a more complex meltwater flux scenario, based on a background freshwater forcing over a longer time period, a rerouting event and a shorter pulse, more intensive, drainage event. Both the magnitude of the meltwater fluxes (Part A), and their duration (Part B) are tested. Finally, a 2.5 SV freshwater flow to the Labrador Sea was added at year 8.47 ka in all simulations in order to simulate the Lake Agassiz outburst¹⁹. The exact date of the Lake Agassiz collapse is uncertain due to uncertainties on reservoir ages of marine cores, which precludes further exploration of the date of the collapse in the simulations in this study.

Data availability

Simulated data for this research is available in the Zenodo database (<https://doi.org/10.5281/zenodo.4282563>) and by contact to the first author. The core data used is available in these in-text data citation references: Morrill et al.¹⁰, Peltier²⁹, Carlson et al.¹⁴, Li et al.²¹, Ullmann et al.¹⁷. Remaining data not present in these sources are available in the supplementary material.

Received: 20 November 2020; Accepted: 17 February 2021

Published online: 09 March 2021

References

- Fettweis, X. *et al.* Reconstructions of the 1900–2015 Greenland ice sheet surface mass balance using the regional climate MAR model. *Cryosphere*. <https://doi.org/10.5194/tc-11-1015-2017> (2017).
- Cazenave, A. How fast are the ice sheets melting?. *Science* **314**, 5803. <https://doi.org/10.1126/science.1133325> (2006).
- Tedesco, M. & Fettweis, X. 21st century projections of surface mass balance changes for major drainage systems of the Greenland ice sheet. *Environ. Res. Lett.* **7**, 4. <https://doi.org/10.1088/1748-9326/7/4/045405> (2012).
- Bakker, P. *et al.* Fate of the Atlantic meridional overturning circulation: Strong decline under continued warming and Greenland melting. *Geophys. Res. Lett.* **43**, 23. <https://doi.org/10.1002/2016GL070457> (2016).
- Swingedouw, D. *et al.* Quantifying the AMOC feedbacks during a $2\times\text{CO}_2$ stabilization experiment with land-ice melting. *Clim. Dyn.* **29**, 5. <https://doi.org/10.1007/s00382-007-0250-0> (2007).
- Golledge, N. R. *et al.* Global environmental consequences of twenty-first-century ice-sheet melt. *Nature* **566**, 7742. <https://doi.org/10.1038/s41586-019-0889-9> (2019).
- Clark, P. U., Pisias, N. G., Stocker, T. F. & Weaver, A. J. The role of the thermohaline circulation in abrupt climate change. *Nature* **415**, 6874. <https://doi.org/10.1038/415863a> (2002).
- Clark, P. U. *et al.* Global climate evolution during the last deglaciation. *Proc. Natl. Acad. Sci.* **109**, 19. <https://doi.org/10.1073/pnas.1116619109> (2012).
- Marson, J. M., Wainer, I., Mata, M. M. & Liu, Z. The impacts of deglacial meltwater forcing on the South Atlantic Ocean deep circulation since the Last Glacial Maximum. *Clim. Past*. **10**, 1723–1734. <https://doi.org/10.5194/cp-10-1723-2014> (2014).
- Alley, R. B. & Ágústsson, A. M. The 8k event: Cause and consequences of a major Holocene abrupt climate change. *Quat. Sci. Rev.* **24**, 10–11. <https://doi.org/10.1016/j.quascirev.2004.12.004> (2005).
- Morrill, C. & Jacobsen, R. M. How widespread were climate anomalies 8200 years ago?. *Geophys. Res. Lett.* **32**, 19. <https://doi.org/10.1029/2005GL023536> (2005).
- Schmidt, G. A. & LeGrande, A. N. The Goldilocks abrupt climate change event. *Quat. Sci. Rev.* **10**, 24. <https://doi.org/10.1016/j.quascirev.2005.01.015> (2005).
- Barber, D. C. *et al.* Forcing of the cold event of 8,200 years ago by catastrophic drainage of Laurentide lakes. *Nature* **400**, 6742. <https://doi.org/10.1038/22504> (1999).
- Clark, P. U. *et al.* Freshwater forcing of abrupt climate change during the last glaciation. *Science* **293**, 5528. <https://doi.org/10.1126/science.1062517> (2001).
- Carlson, A. E., Clark, P. U., Haley, B. A. & Klinkhammer, G. P. Routing of western Canadian Plains runoff during the 8.2 ka cold event. *Geophys. Res. Lett.* **36**, 14. <https://doi.org/10.1029/2009GL038778> (2009).
- Carlson, A. E. *et al.* Rapid early Holocene deglaciation of the Laurentide ice sheet. *Nat. Geosci.* **1**, 9. <https://doi.org/10.1038/ngeo285> (2008).
- Gregoire, L. J., Payne, A. J. & Valdes, P. J. Deglacial rapid sea level rises caused by ice-sheet saddle collapses. *Nature* **487**, 7406. <https://doi.org/10.1038/nature11257> (2012).
- Ullman, D. J. *et al.* Final Laurentide ice-sheet deglaciation and Holocene climate-sea level change. *Quat. Sci. Rev.* <https://doi.org/10.1016/j.quascirev.2016.09.014> (2016).
- Clarke, G. K., Leverington, D. W., Teller, J. T. & Dyke, A. S. Paleohydraulics of the last outburst flood from glacial Lake Agassiz and the 8200BP cold event. *Quat. Sci. Rev.* **23**, 3–4. <https://doi.org/10.1016/j.quascirev.2003.06.004> (2004).

20. Carlson, A. E. *et al.* Surface-melt driven Laurentide Ice Sheet retreat during the early Holocene. *Geophys. Res. Lett.* **36**, 24. <https://doi.org/10.1029/2009GL040948> (2009).
21. Meissner, K. J. & Clark, P. U. Impact of floods versus routing events on the thermohaline circulation. *Geophys. Res. Lett.* **33**, 15. <https://doi.org/10.1029/2006GL026705> (2006).
22. Li, Y. X., Törnqvist, T. E., Nevitt, J. M. & Kohl, B. Synchronizing a sea-level jump, final Lake Agassiz drainage, and abrupt cooling 8200 years ago. *Earth Planet. Sci. Lett.* **315**, 41–50. <https://doi.org/10.1016/j.epsl.2011.05.034> (2012).
23. Morrill, C. *et al.* Large sensitivity to freshwater forcing location in 8.2 ka simulations. *Paleoceanography* **29**, 10. <https://doi.org/10.1002/2014PA002669> (2014).
24. Wagner, A. J. *et al.* Model support for forcing of the 8.2 ka event by meltwater from the Hudson Bay ice dome. *Clim. Dyn.* **41**, 11–12. <https://doi.org/10.1007/s00382-013-1706-z> (2013).
25. Wiersma, A. P., Renssen, H., Goosse, H. & Fichefet, T. Evaluation of different freshwater forcing scenarios for the 8.2 ka BP event in a coupled climate model. *Clim. Dyn.* **27**, 7–8. <https://doi.org/10.1007/s00382-006-0166-0> (2006).
26. Aguiar, W. *et al.* Freshwater forcing control on early-Holocene South American monsoon. *Quat. Sci. Rev.* <https://doi.org/10.1016/j.quascirev.2020.106498> (2020).
27. Cheng, W., Chiang, J. C. & Zhang, D. Atlantic meridional overturning circulation (AMOC) in CMIP5 models: RCP and historical simulations. *J. Clim.* **26**, 18. <https://doi.org/10.1175/JCLI-D-12-00496.1> (2013).
28. Weaver, A. J. *et al.* Stability of the Atlantic meridional overturning circulation: A model intercomparison. *Geophys. Res. Lett.* **39**, 20. <https://doi.org/10.1029/2012GL053763> (2012).
29. Van den Broeke, M. R. *et al.* On the recent contribution of the Greenland ice sheet to sea level change. *Cryosphere*. <https://doi.org/10.5194/tc-10-1933-2016> (2016).
30. Peltier, W. R. Global glacial isostasy and the surface of the ice-age Earth: The ICE-5G (VM2) model and GRACE. *Annu. Rev. Earth Planet. Sci.* <https://doi.org/10.1146/annurev.earth.32.082503.144359> (2004).
31. Lawrence, T. *et al.* Relative sea-level data from southwest Scotland constrain meltwater-driven sea-level jumps prior to the 8.2 kyr BP event. *Quat. Sci. Rev.* <https://doi.org/10.1016/j.quascirev.2016.06.013> (2016).
32. Bradley, S. L. *et al.* An improved glacial isostatic adjustment model for the British Isles. *J. Quat. Sci.* **26**, 5. <https://doi.org/10.1002/jqs.1481> (2011).
33. Hijma, M. P. & Cohen, K. M. Timing and magnitude of the sea-level jump precluding the 8200 yr event. *Geology* **38**, 3. <https://doi.org/10.1130/G30439.1> (2010).
34. Streif, H. Sedimentary record of Pleistocene and Holocene marine inundations along the North Sea coast of Lower Saxony, Germany. *Quat. Sci. Rev.* **112**, 1. [https://doi.org/10.1016/S1040-6182\(03\)00062-4](https://doi.org/10.1016/S1040-6182(03)00062-4) (2004).
35. Smith, D. E. *et al.* Sea level rise and submarine mass failures on open continental margins. *Quat. Sci. Rev.* <https://doi.org/10.1016/j.quascirev.2013.10.012> (2013).
36. Matero, I. S. O. *et al.* The 8.2 ka cooling event caused by Laurentide ice saddle collapse. *Earth Planet. Sci. Lett.* <https://doi.org/10.1016/j.epsl.2017.06.011> (2017).
37. LeGrande, A. N. *et al.* Consistent simulations of multiple proxy responses to an abrupt climate change event. *Proc. Natl. Acad. Sci.* **103**, 4. <https://doi.org/10.1073/pnas.0510095103> (2006).
38. Kleiven, H. K. F. *et al.* Reduced North Atlantic deep water coeval with the glacial Lake Agassiz freshwater outburst. *Science* **319**, 5859. <https://doi.org/10.1126/science.1148924> (2008).
39. Aschwanden, A. *et al.* Contribution of the Greenland Ice Sheet to sea level over the next millennium. *Sci. Adv.* **5**, 6. <https://doi.org/10.1126/sciadv.aav9396> (2019).
40. Lenaerts, J. T. *et al.* Representing Greenland ice sheet freshwater fluxes in climate models. *Geophys. Res. Lett.* **42**, 15. <https://doi.org/10.1002/2015GL064738> (2015).
41. Weaver, A. J. *et al.* The UVic Earth System Climate Model: Model description, climatology, and applications to past, present and future climates. *Atmos. Ocean* **39**, 4. <https://doi.org/10.1080/07055900.2001.9649686> (2001).
42. Brennan, C. E., Weaver, A. J., Eby, M. & Meissner, K. J. Modelling oxygen isotopes in the University of Victoria Earth System Climate Model for pre-industrial and Last Glacial Maximum conditions. *Atmos. Ocean* **50**, 4. <https://doi.org/10.1080/07055900.2012.707611> (2012).
43. Brennan, C. E. *et al.* Impact of sea ice variability on the oxygen isotope content of seawater under glacial and interglacial conditions. *Paleoceanography* **28**, 3. <https://doi.org/10.1002/palo.20036> (2013).
44. Bagniewski, W., Meissner, K. J., Menviel, L. & Brennan, C. E. Quantification of factors impacting seawater and calcite $\delta^{18}\text{O}$ during Heinrich Stadials 1 and 4. *Paleoceanography* **30**, 7. <https://doi.org/10.1002/2014PA002751> (2015).
45. Bagniewski, W., Meissner, K. J. & Menviel, L. Exploring the oxygen isotope fingerprint of Dansgaard-Oeschger variability and Heinrich events. *Quat. Sci. Rev.* <https://doi.org/10.1016/j.quascirev.2017.01.007> (2017).
46. Yeung, N. K. H., Menviel, L., Meissner, K. J. & Sikes, E. Assessing the spatial origin of meltwater pulse 1A using oxygen-isotope fingerprinting. *Paleocean. Paleoclim.* **34**, 12. <https://doi.org/10.1029/2019PA003599> (2019).
47. Morrill, C. *et al.* Proxy benchmarks for intercomparison of 8.2 ka simulations. *Clim. Past*. **9**, 1. <https://doi.org/10.5194/cp-9-423-2013> (2013).
48. Bemis, B. E. *et al.* Reevaluation of the oxygen isotopic composition of planktonic foraminifera: Experimental results and revised paleotemperature equations. *Paleoceanography* **13**, 2. <https://doi.org/10.1029/98PA00070> (1998).
49. Kim, S. T. & O'Neil, J. R. Equilibrium and nonequilibrium oxygen isotope effects in synthetic carbonates. *Geochim. Cosmochim. Acta.* **61**, 16. [https://doi.org/10.1016/S0016-7037\(97\)00169-5](https://doi.org/10.1016/S0016-7037(97)00169-5) (1997).
50. Diebold, F. X. & Mariano, R. S. Comparing predictive accuracy. *J. Bus. Econ. Stat.* **20**, 1. <https://doi.org/10.1198/073500102753410444> (2002).
51. Briggs, R. D. & Tarasov, L. How to evaluate model-derived deglaciation chronologies: A case study using Antarctica. *Quat. Sci. Rev.* <https://doi.org/10.1016/j.quascirev.2012.11.021> (2013).
52. Fisher, D. A. *et al.* Penny ice cap cores, Baffin Island, Canada, and the Wisconsinan Foxe Dome connection: Two states of Hudson Bay ice cover. *Science* **279**, 5351. <https://doi.org/10.1126/science.279.5351.692> (1998).
53. Remenda, V. H., Cherry, J. A. & Edwards, T. W. D. Isotopic composition of old ground water from Lake Agassiz: Implications for late Pleistocene climate. *Science* **266**, 5193. <https://doi.org/10.1126/science.266.5193.1975> (1994).

Acknowledgements

This work is a part of the activities from the Brazilian High Latitudes Oceanography Group (GOAL) and the Brazilian National Institute of Science and Technology of the Cryosphere (INCT-CRIOSFERA; 573720/2008-8, 465680/2014-3, FAPERGS 17/2551-0000518-0). The GOAL is currently funded by the Brazilian Antarctic Program (PROANTAR) through the Brazilian Ministry of the Environment (MMA), the Brazilian Ministry of Science, Technology, Innovation and Communication (MCTIC), and the Council for Research and Scientific Development of Brazil (CNPq; 442628/2018-8, CAPES AUXPE 1995/2014). W. Aguiar acknowledges the financial support from the CAPES Foundation, and the Fulbright association for promoting the scientific interchange required by this work. M. M. Mata acknowledges CNPq grant nos. 306896/2015-0. K. J. Meissner acknowledges

funding from the Australian Research Council (DP180100048, DP18012357). L. Prado acknowledges the INCT-CRIOSFERA (88887.495715/2020-00), and I. Wainer acknowledges the São Paulo Research Foundation (2018/14789-9; 2019/08247-1) and CNPq (300970/2018-8). All authors acknowledge Dr. James Scourse for the valuable review.

Author contributions

The respective contribution of each author to the manuscript is listed below. The descriptions here depicted are accurate and agreed upon by all authors. All authors approved the submitted version of this manuscript. W.A.: conceptualization, methodology, validation, formal analysis, investigation, data curation, writing—original draft, writing—review and editing, visualization. L.F.P.: methodology, software, validation, formal analysis, investigation, writing—review and editing, visualization. I.W.: methodology, validation, formal analysis, writing—review and editing, visualization, resources, supervision. A.E.C., A.M., K.J.M.: conceptualization, methodology, validation, formal analysis, writing—review and editing, visualization, resources, supervision. M.M.M.: conceptualization, methodology, validation, formal analysis, writing—review and editing, visualization, resources, supervision, project administration, funding acquisition.

Competing interests

The authors declare no competing interests.

Additional information

Supplementary Information The online version contains supplementary material available at <https://doi.org/10.1038/s41598-021-84709-5>.

Correspondence and requests for materials should be addressed to W.A.

Reprints and permissions information is available at www.nature.com/reprints.

Publisher's note Springer Nature remains neutral with regard to jurisdictional claims in published maps and institutional affiliations.



Open Access This article is licensed under a Creative Commons Attribution 4.0 International License, which permits use, sharing, adaptation, distribution and reproduction in any medium or format, as long as you give appropriate credit to the original author(s) and the source, provide a link to the Creative Commons licence, and indicate if changes were made. The images or other third party material in this article are included in the article's Creative Commons licence, unless indicated otherwise in a credit line to the material. If material is not included in the article's Creative Commons licence and your intended use is not permitted by statutory regulation or exceeds the permitted use, you will need to obtain permission directly from the copyright holder. To view a copy of this licence, visit <http://creativecommons.org/licenses/by/4.0/>.

© The Author(s) 2021